10TH TO MEETING
10/15/2013

Space-time evolution of crustal deformation from GPS data: Principal Component Analysis (PCA), Independent Comopnent Analysis (ICA) and the L'Aquila earthquake (central Italy)

A. Gualandi
adriano.gualandi@bo.ingv.it

Abstract

Geodetic time series data are usually studied through classical statistical techniques, that is decomposing them into different deterministic signals. Recently, new techniques have been developed and applied to geodetic data, in order to extract as much information as possible from them. An example is the Principal Component Analysis (PCA), used both to detect network errors in GPS data (such as the Common Mode Error, CME, see Dong et al., 2006), and to identify geophysical signals common to a certain region. The latter approach is particularly useful for understanding geophysical processes, and the PCA-based Inversion Method (PCAIM, see Kositsky and Avouac, 2010) is a good realization of this concept. I used this method to analyze the GPS data of the 2009 L'Aquila earthquake (central Italy). A strong limitation of the PCA is that it is not able to separate multiple mixed sources. In other words, the PCA technique is not effective in treating the so-called Blind Source Separation (BSS) problem. For this goal, it reveals to be an efficient technique the Independent Component Analysis (ICA). The objective of my project is to modify the decomposition step of the PCAIM code. In particular, I want to introduce the possibility to perform an ICA decomposition, with the goal to detect and separate multiple sources of signal.

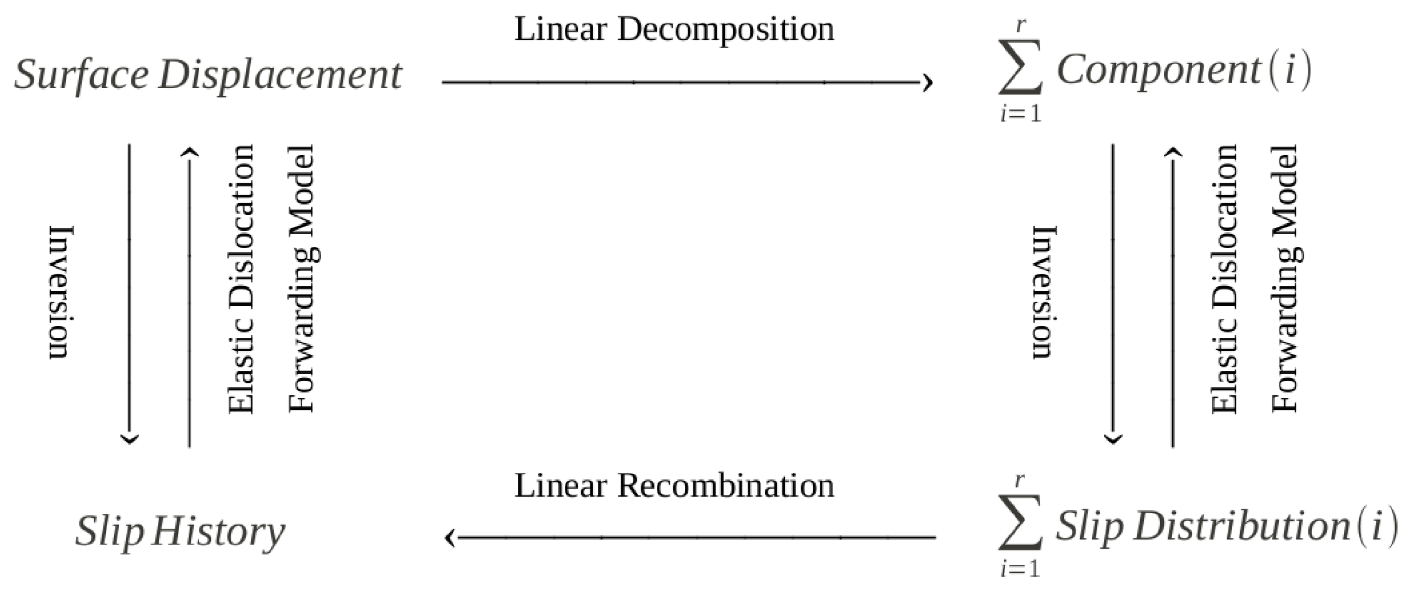

Fig. 1: Diagram showing principle of PCAIM (Kositsky and Avouac, 2010). PCAIM decomposes displacement data into sum of so-called principal components. Each of components is individually modeled and translated into a corresponding principal slip distribution model. Note that the slip model associated with any one particular component does not have any particular physical significance.

1 - The L'Aquila earthquake

The mainshock of the 2009 L'Aquila earthquake occurred on a NE-trending, SW-ward dipping normal fault, and activated a complex system of SW-dipping segments. The most relevant are Paganica and Campotosto faults (see Fig. 2). We use the relocated aftershock catalogue of Chiaraluce et al. (2011) to define a suite of fault model geometries for the Paganica and Campotosto faults to be used in the coseismic and postseismic slip inversions, and test the sensitivity of GPS data to the use of increasingly complex fault geometries, using as a benchmark for the Paganica fault its geodetic solution. We also consider the possibility that rake constraints affect the slip distributions, since published results did not investigated this issue.

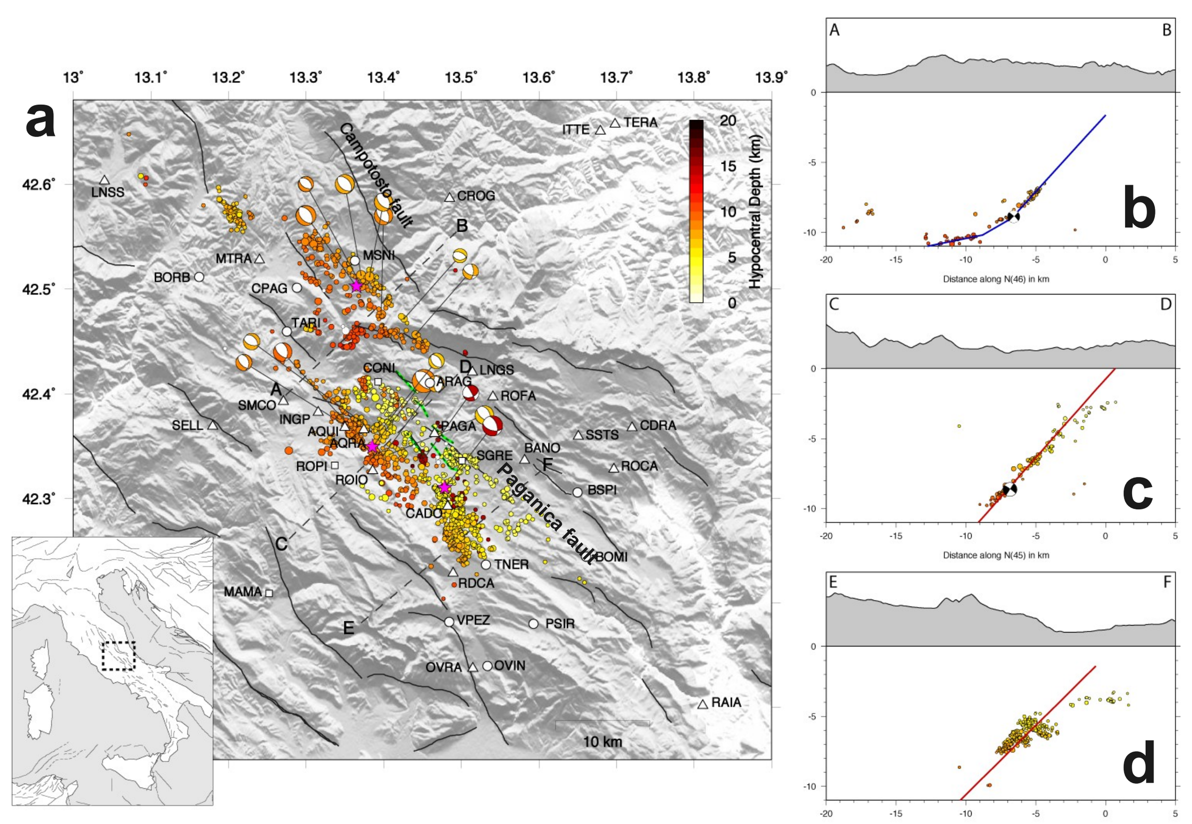

Fig. 1: a) Map of the region involved in the seismic sequence with aftershocks (colored circles, Chiaraluce et al., 2011), focal mechanisms (Pondrelli et al., 2009), mainshock and the two most relevant aftershocks (purple stars), GPS stations used (white circles / squares / triangles for coseismic / postseismic / both inversions), active faults (black lines) and surface ruptures (green lines). Dashed lines are the sections reported in panels b, c and d. b) Section A-B of panel a. The focal mechanism corresponds to the April 9 aftershock. Blue line is the section of the Campotosto geometry. The focal mechanism (c) represents the mainshock. c-d) Sections C-D and E-F of panel a. Red lines are the sections of the Paganica geometry.

2 - GPS data

The input GPS time-series have been obtained by analyzing raw data with the GAMIT/GLOBK software, as described in Serpelloni et al. (2012). We use a PCA method to estimate spatially-correlated common mode noise errors (CME) for a wider area in the Euro-Mediterranean, using a set of 640 cGPS stations, while excluding those in the epicentral area and its surroundings. Filtering the time-series provides a significant gain in the signal-to-noise ratio, which is particularly important for studying moderate earthquakes. For the coseismic slip distribution we use 67 GPS stations; to study the postseismic signal we use 27 GPS stations that recorded continuously after the mainshock.

References

Boatwright and Cocco, 1996, *J, Geophys. Res.*
Chiaraluce et al., 2011, *J, Geophys. Res.*
Dong et al., 2006, *J, Geophys. Res.*
Kositsky and Avouac, 2010, *J, Geophys. Res.*
Marone et al., 1991, *J, Geophys. Res.*
Okada, 1985, *Bull. Seism. Soc. Am.*
Perfettini and Ampuero, 2008, *J, Geophys. Res.*
Pondrelli et al., 2010, *Geophys. J. Int.*
Scuderi et al., 2013, *Earth and Pl. Sc. Lett.*
Serpelloni et al., 2012, *Geophys. J. Int.*

3 - Results

We reproduce the original data adopting one principal component for the coseismic deformation and two for the postseismic (see Fig. 3). We invert for both coseismic and postseismic slips using the Okada (1985) formulation. We assume a shear modulus of 30 GPa and a Poisson ratio of 0.25. In both cases we estimate the regularization parameter γ using the L-curve method considering the roughness of the model and the reduced χ^2.

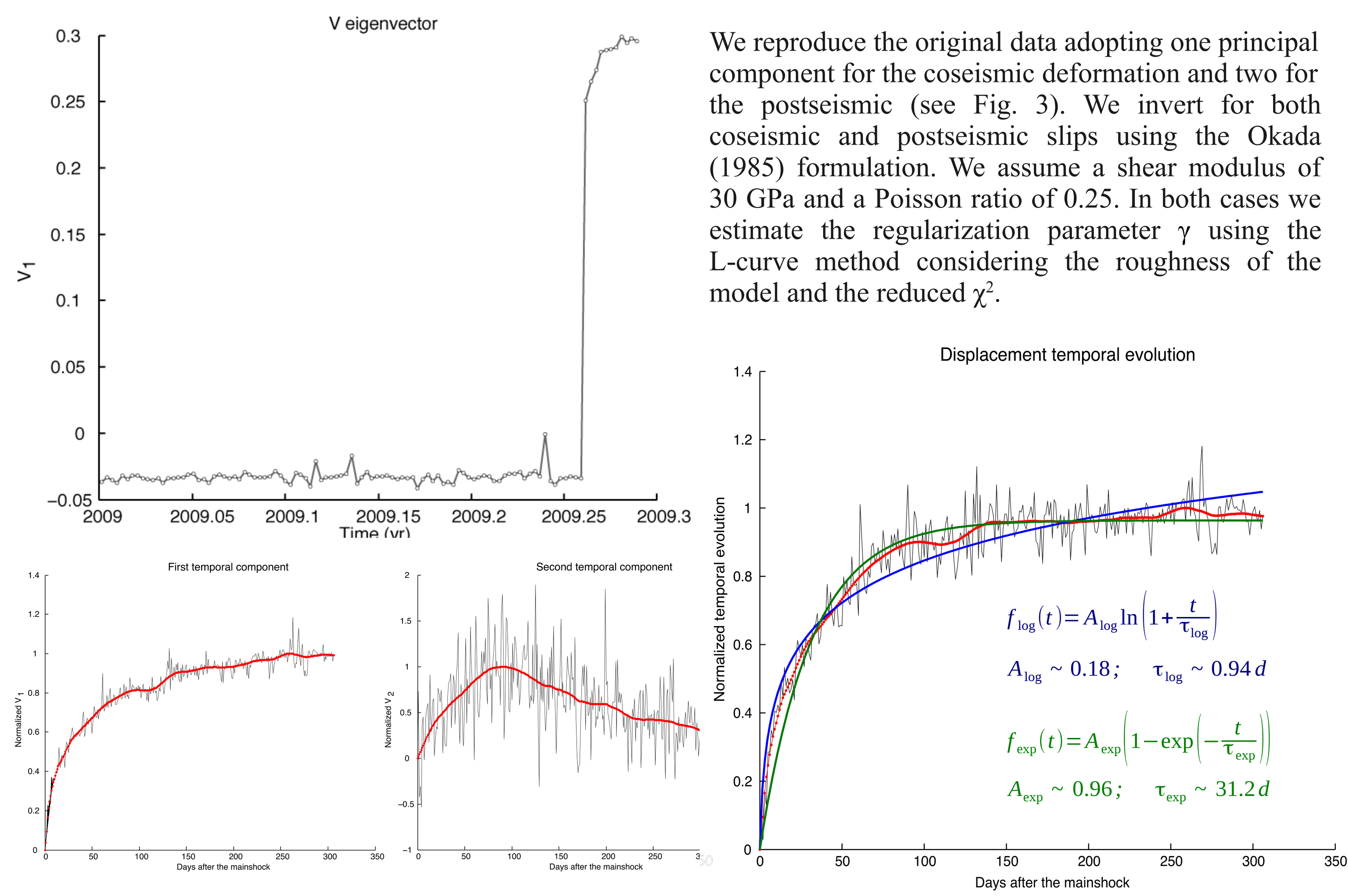

Fig. 3: a) Temporal eigenvector for the coseismic decomposition. b-c) First and second temporal eigenvectors for the postseismic decomposition. Red lines are obtained filtering high frequency signal. d) Displacement temporal evolution for the postseismic decomposition. Blue line is the best logarithmic fit and green line is the best exponential fit. The best parameters are estimated with an unconstrained nonlinear minimization of the sum of squared residuals (SSR).

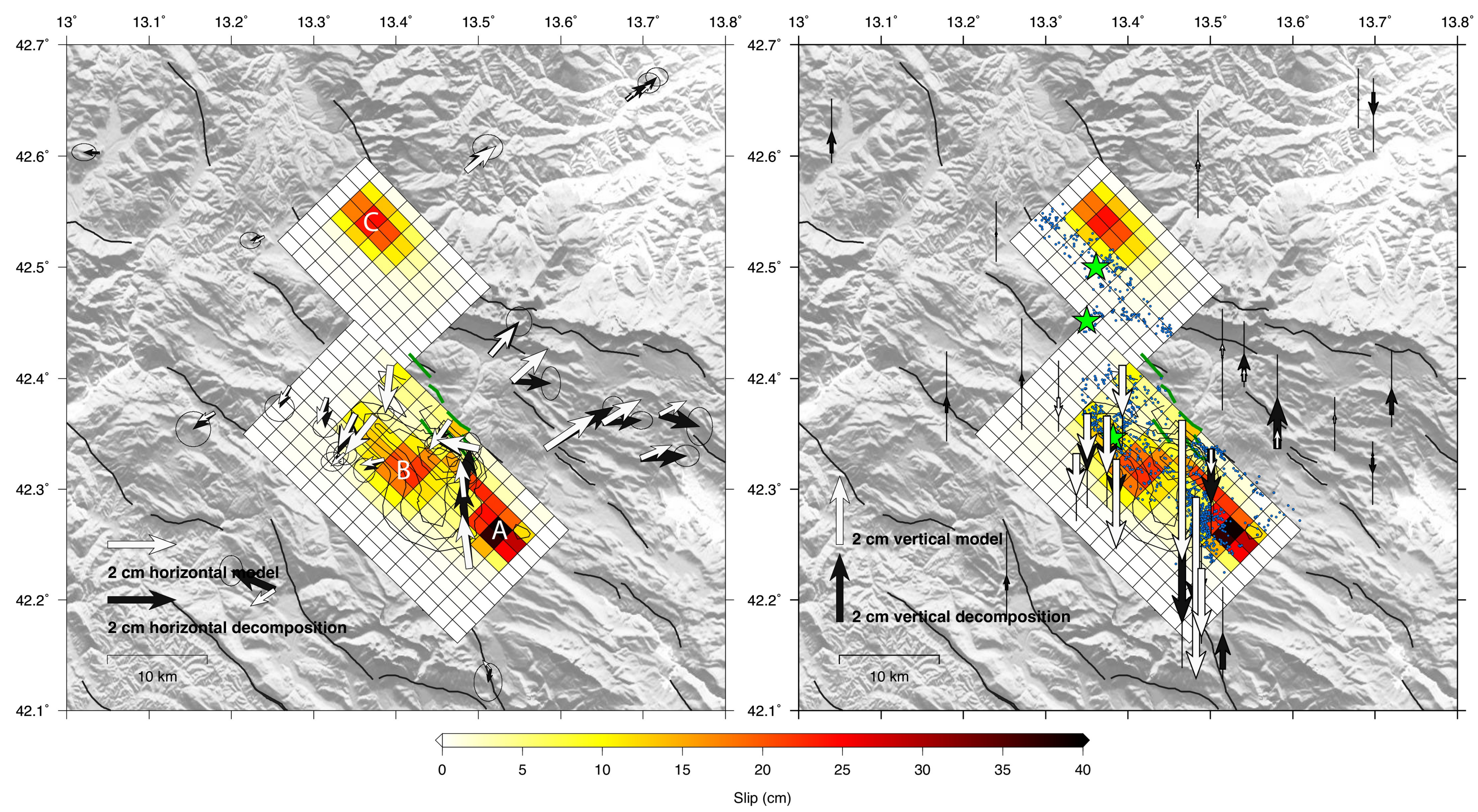

Fig. 4: Best post-seismic slip model. Contouring lines indicate co-seismic constant slip regions of the best model, starting from 20 cm to the maximum value, stepping every 20 cm. a) and b) show horizontal and vertical cumulative displacements, respectively. Capital letters A, B and C indicate the afterslip regions. Green stars show the location of the mainshock (on the Paganica fault) and the two aftershocks of the 9th of April and 22nd of June. Blue dots indicate the aftershock distribution.

Perfettini and Ampuero (2008):

$$\Delta CFF=(a-b)\sigma\log\frac{\beta}{V_{pl}} \qquad \text{for } \Delta CFF>0$$

$\Delta CFF_A\in[0.3;2.1]$ MPa	positive variation of Coulomb stress in region A
$\Delta CFF_C\sim 0.03$ MPa	positive variation of Coulomb stress in region C
a,b	rate- and state- frictional parameters
$\beta\in[0.3;4.3]$ cm/d	starting postseismic sliding velocity
$\sigma\in[40;100]$ MPa	effective normal stress
$V_{pl}\in[0.2;3]$ mm/yr	loading plate velocity (geological and geodetic)

Marone et al. (1991):

$$\delta(t)-\delta(t_1)\approx\alpha\ln\left[\frac{\alpha+\beta t}{\alpha+\beta t_1}\right] \qquad \text{for} \quad t_1\leqslant t\ll t_d=\frac{\alpha}{V_{pl}}$$

$\alpha=\frac{(a-b)\sigma}{k}=V_{pl}t_d$	characteristic slip
k	stiffness of the spring in the fault analog model
σ	effective normal stress
V_{pl}	loading plate velocity (geological and geodetic)
t_d	characteristic decay time
$\beta=V_+$	starting postseismic sliding velocity

We find a–b values in the range 10^{-4}-10^{-3}, with the most frequent value of the order of 10^{-3}, in agreement with studies of fault rocks typical of these regions at elevated temperatures and under fluid-saturated conditions (Scuderi et al., 2013). Small a–b values, such as 10^{-3} (Marone et al., 1991), characterize fault regions where transitions between velocity-weakening (a–b < 0) and velocity-strengthening (a–b > 0) occur. These regions may undergo both afterslip and aftershocks during the post-seismic phase (Boatwright and Cocco, 1996). The M_W 4.4 aftershock occurred 77 days after the mainshock (see Figures 4 and 5b) is a seismic event located on the Campotosto fault below the region undergoing afterslip. The fault region where the aftershock occurred was affected by a negligible coseismic stress change due to the L'Aquila mainshock (ΔCFF<0.01 MPa). Instead, it experienced a Coulomb stress increase of 0.06 MPa due to afterslip on the Campotosto fault, and it was slightly unloaded by afterslip on the Paganica fault, resulting in a net increase of stress after 77 days of post-seismic stage of 0.05 MPa.

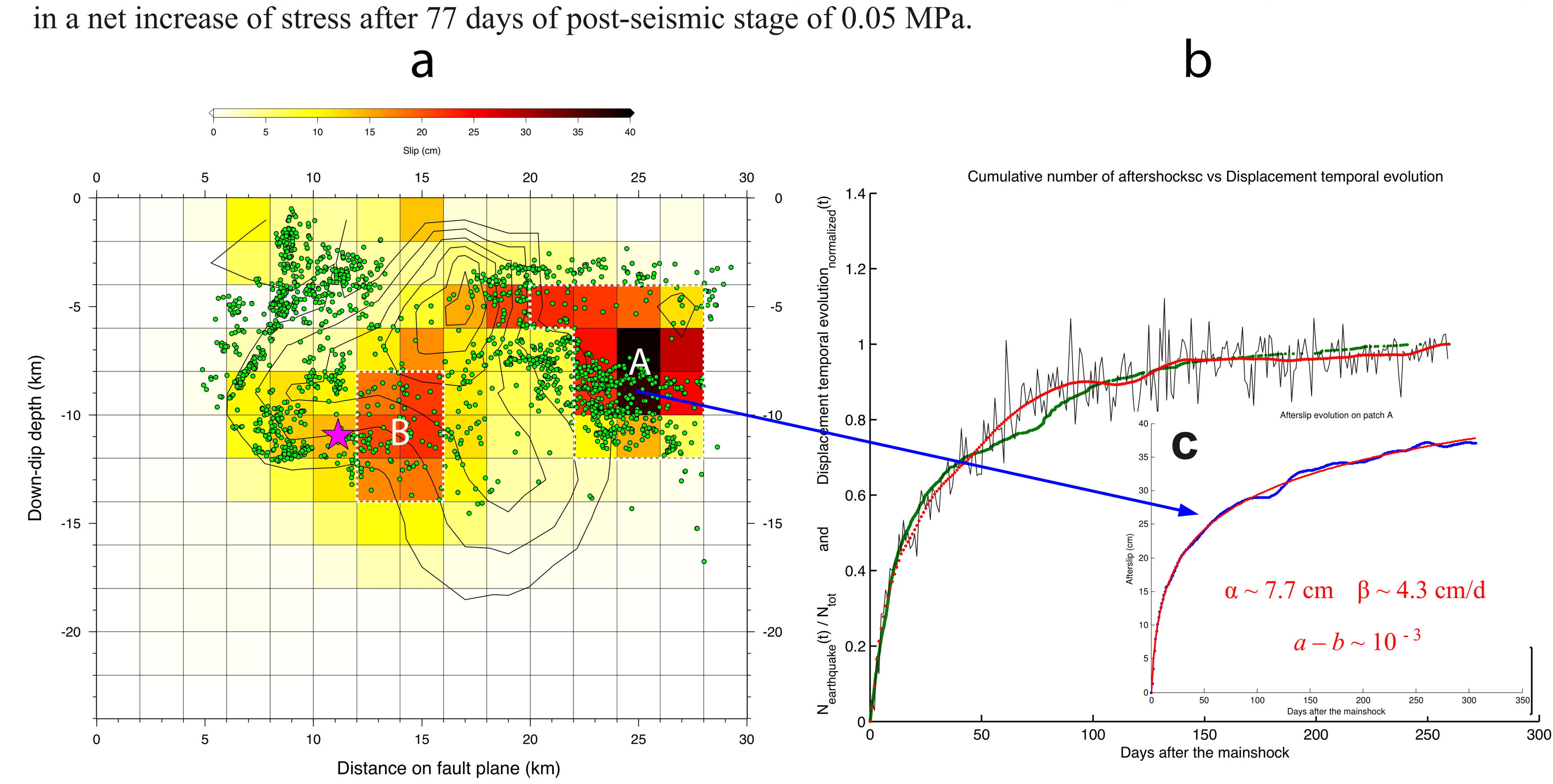

Fig. 5: a) Afterslip distribution on the Paganica fault plane. Green dots are the projected aftershocks. Continuous lines represent the coseismic slip, as in Fig. 4. The purple star localizes the main shock event. Capital letters A and B indicate the afterslip regions. Region A is used for the calculation of the frictional parameter a–b. b) Temporal evolution of afterslip and GPS postseismic displacement (red line, as in Figure 3d) and cumulative number of aftershocks (green line). At 77 days after the mainshock, in correspondence to the 22nd of June aftershock, there is a sudden increase of the cumulative number of aftershocks. c) Afterslip history of the main afterslip patch experiencing coseismic stress increase. The blue dots represent the afterslip deduced from the inversion of GPS data; the red line represents the frictional model. The parameter values α and β have been obtained through an unconstrained nonlinear minimization of the sum of squared residuals.

4 - ICA

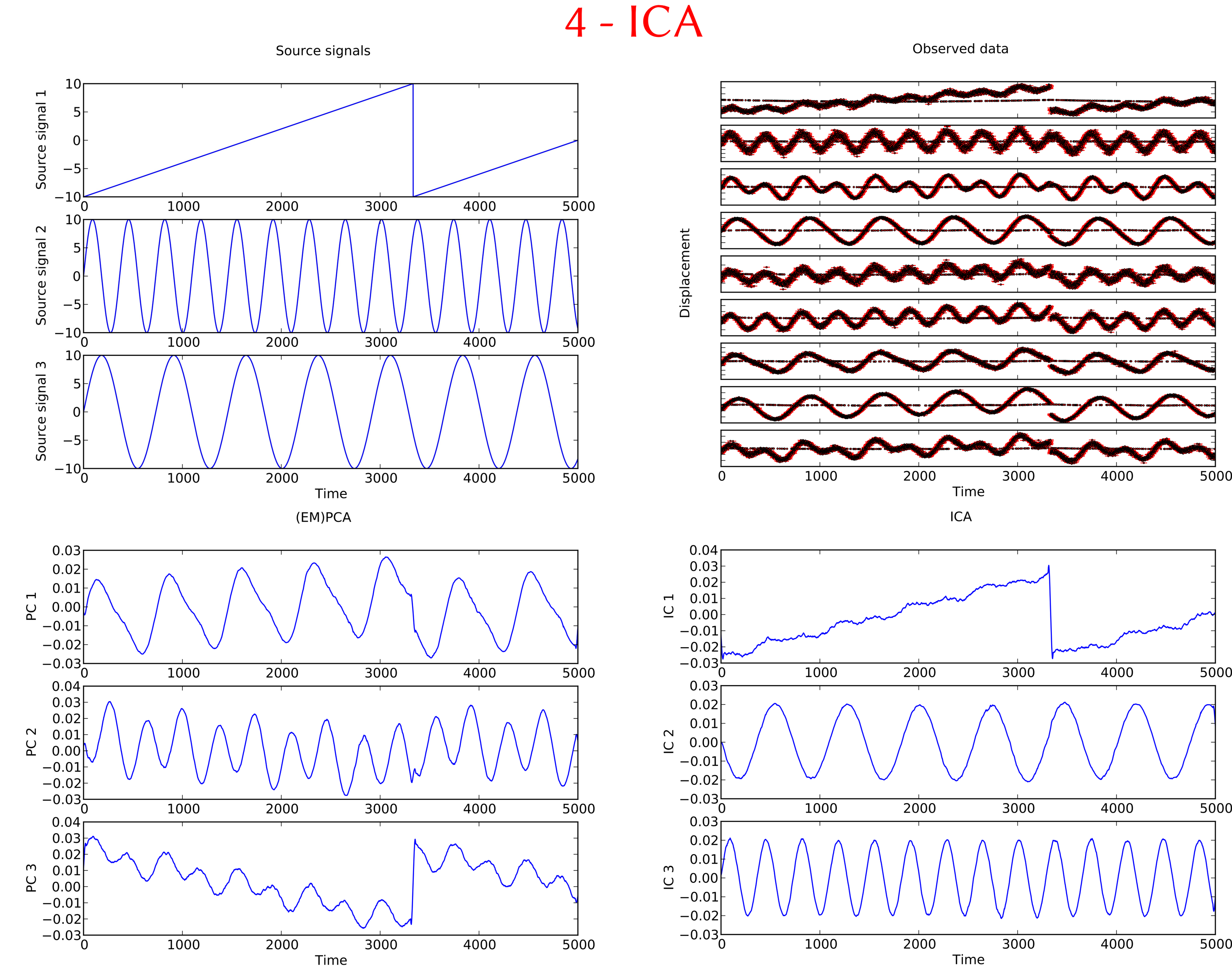

Fig. 6: Schematic representation of the ICA decomposition. a) Source signals. b) Observed data. c) Reconstructed temporal functions through PCA. d) Reconstructed sources through ICA.